Volume 13 | Number 7 | 31 March 2026

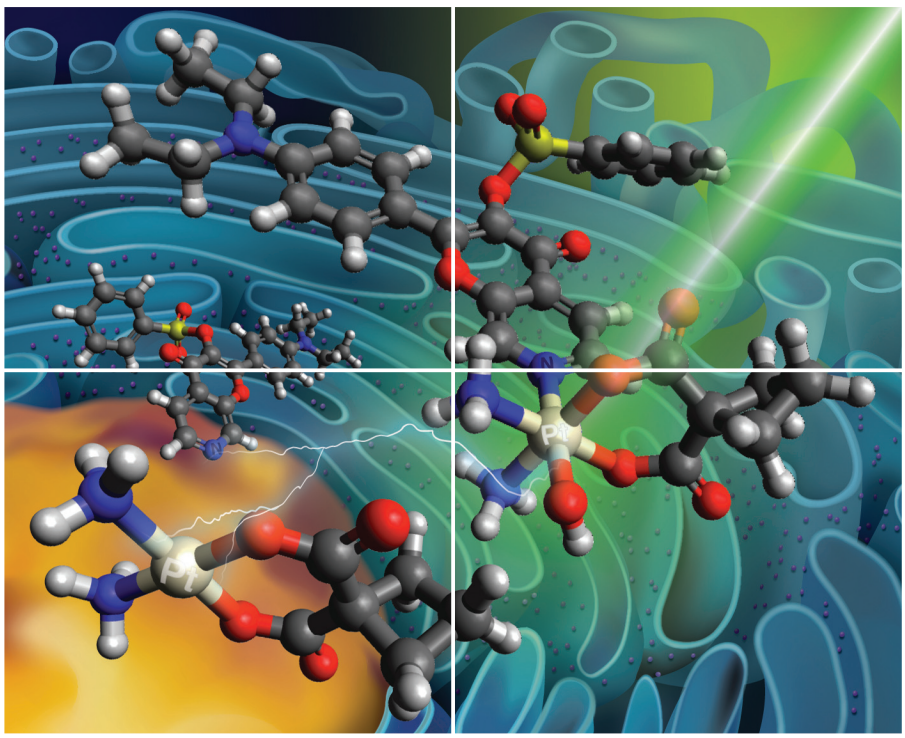

# INORGANIC CHEMISTRY

## FRONTIERS

CCS 中国化学会 CHINESE CHEMICAL SOCIETY

PEKING UNIVERSITY 1898

ROYAL SOCIETY OF CHEMISTRY

rsc.li/frontiers-inorganic

INORGANIC CHEMISTRY
FRONTIERS

RESEARCH ARTICLE

View Article Online
View Journal | View Issue



Cite this: *Inorg. Chem. Front.*, 2026, **13**, 2835

# Flavoplatins: photoactivated platinum(IV) prodrugs bearing axial N-donors that trigger pyroptosis and reduce drug resistance

Qiyuan Zhou,[a,b] Nang-Hei Chu,[a] Jiaqian Xu,[a,b] Kwok-Chung Law[a] and Guangyu Zhu *[a,b]

Photoactivated Pt(IV) anticancer prodrugs derived from clinical Pt(II) drugs have garnered significant attention in recent years, with O-donor ligands being the most commonly used photosensitive axial ligands. N-donor ligands, however, such as N-heteroaromatics, offer the potential to enhance the ligand-to-metal charge transfer (LMCT) of Pt(IV) complexes, thereby improving their photochemical properties. Herein, we report a series of green-light activable Pt(IV) prodrugs bearing N-donor axial ligands, designated flavoplatins, based on carboplatin and oxaliplatin. These prodrugs, functionalized with flavonol derivatives as photosensitive axial ligands, enabled rapid reduction under light irradiation to release Pt(II) drugs and the corresponding axial ligands. Flavoplatins **3a** and **3b** demonstrated exceptional photocytotoxicity, exhibiting at least a 27-fold increase in effectiveness compared to carboplatin in both Pt-sensitive and Pt-resistant cancer cells. Additionally, both complexes efficiently accumulated in the endoplasmic reticulum and quickly induced pyroptosis *via* the NLRP-3/caspase-1/GSDMD pathway. This study underscores a promising alternative strategy for designing novel photoactivatable Pt(IV) prodrugs containing axial N-donors with enhanced therapeutic potential, particularly for targeting specific cellular pathways and reducing drug resistance.

Received 13th January 2026,
Accepted 13th February 2026

DOI: 10.1039/d6qi00078a

rsc.li/frontiers-inorganic



## Introduction

Flavonoids are an important class of natural products found in fungi and plants,[1,2] featuring a heterobicyclic structure with a phenyl group substituted at the 2-position.[3] Based on structural variations, flavonoids are categorized into several subgroups, including flavonols,[4] which are extensively studied for their anticancer properties.[5,6] Among the notable flavonols, quercetin–a dietary compound present in many fruits and vegetables–has shown broad-spectrum anticancer activity and progressed to phase II clinical trials.[7,8] Other flavonols have been reported to actively disrupt cell cycles, regulate signaling enzymes, and induce apoptosis in cancer cells.[9–11] Flavonols also exhibit endoplasmic reticulum (ER)-targeting properties, largely due to their strong hydrophobic interactions with the ER.[12,13] Further modifications to flavonols, such as the addition of sulfonated substituent groups, have been shown to enhance their ER-targeting ability.[14] Additionally, the excited-state intramolecular proton-transfer (ESIPT) properties of flavonols result in strong and long-wavelength emissions in their excited tautomeric forms,[15] enabling their application in whole-cell imaging and organelle probing.[12,16]

Since the discovery of cisplatin as the first anticancer platinum drug, significant efforts have been devoted to developing novel Pt-based anticancer agents.[17] For example, Pt(IV) prodrugs derived from Pt(II) drugs including cisplatin, carboplatin, and oxaliplatin have been widely reported.[18–21] A critical aspect of designing these prodrugs is their reduction to release the active Pt(II) species, which drives their anticancer activity.[22–24] O-donor ligands are commonly employed as axial ligands to confer multifunctionality on Pt(IV) anticancer prodrugs based on clinical Pt(II) drugs.[21,25,26] In contrast, N-donor ligands are less commonly reported. Notable examples include amidates and pyridines, which can also coordinate axially to the Pt(IV) center through either oxidation of Pt(II) drugs or ligand exchange reactions involving labile axial ligands.[27–29] It is noteworthy that axial amidates and pyridine ligands can be efficiently released during the reduction of Pt(IV) complexes.[27–29] This observation highlights axial *N*-coordination as a promising strategy for designing Pt(IV) anticancer prodrugs. Furthermore, these synthetic approaches allow diverse modifications of the axial ligands, enabling the fine-tuning of reduction profiles, conjugation

[a]*Department of Chemistry, City University of Hong Kong, 83 Tat Chee Ave, Kowloon Tong, Hong Kong SAR, P. R. China. E-mail: guangzhu@cityu.edu.hk*
[b]*City University of Hong Kong Shenzhen Research Institute, Shenzhen 518057, P. R. China*

with bioactive molecules,[29] or incorporation of photosensitive ligands.

Photoactivation has recently emerged as a controllable method for activating Pt(IV) prodrugs to enhance their anticancer potency and selectivity.[30–37] These prodrugs exhibit significant cytotoxicity and additional bioactivities upon irradiation, such as generating reactive oxygen species (ROS) and inducing photo-oxidation of cellular components.[37–39] Currently, most photosensitive axial ligands in clinical Pt(II) drug-based Pt(IV) complexes are conjugated *via O*-coordination, while N-coordinated axial ligands are rarely reported. Intriguingly, N-donor ligands exhibit ligand-to-metal charge transfer (LMCT) properties, which narrow the energy gap between the ground state and the excited state, destabilizing the Pt–N bond upon excitation.[40] Consistent with this behavior, azido, pyridine, or ethylenediamine N-donors enable LMCT-mediated activation of Pt(IV) complexes under short-wavelength visible light.[31,32,41] Among these, pyridine–as an N-heteroaromatic scaffold–offers synthetic versatility for conjugation with photosensitive molecules. More broadly, N-heteroaromatic ligands exhibit strong electron transfer abilities, enhance photosensitivity, and are widely utilized in photocatalytic metal complexes.[42] As a result, the LMCT bands of Pt(IV) complexes containing N-heteroaromatic ligands are significantly red-shifted,[43] enabling activation by longer wavelengths of light. This property enhances the photosensitivity of Pt(IV) prodrugs and facilitates the adjustment of activation wavelength.

Herein, we report the design and synthesis of a series of green-light-activable Pt(IV) prodrugs featuring flavonol-derived N-donor axial ligands. Photocytotoxicity assays demonstrated a significant increase in activity under irradiation compared to dark conditions, highlighting their light-triggered therapeutic potential. Notably, flavoplatins preferentially localized to the ER and induced pyroptosis through well-characterized pathways, which contributed to reducing platinum drug resistance. This study introduces a novel approach to designing photoactivatable Pt(IV) prodrugs bearing axial N-donors and highlights the potential of such agents to achieve enhanced anticancer potency and selectivity through light-controlled activation.

## Results and discussion

Previously, we reported a synthetic method for coordinating N-heteroaromatic ligands to Pt(IV) complexes utilizing a ligand exchange reaction with the axial halogen ligands of Pt(IV) complexes.[29] Building on this approach, flavonol analogs bearing a pyridinyl moiety were rationally designed as axial ligands for Pt(IV) complexes and synthesized following the previously reported method.[29] In brief, 3-hydroxy-4-acetylpyridine underwent a condensation reaction with 4-diethylaminobenzaldehyde under basic conditions, yielding a chalcone-derived intermediate. After neutralization with nitric acid, hydrogen peroxide solution was directly added to the reaction mixture, oxidizing the chalcone derivative to produce the ligand **flav-1** (Scheme S1A). Ligands **flav-2** and **flav-3** were subsequently obtained by reacting **flav-1** with acetic anhydride and benzenesulfonyl chloride, respectively (Schemes S1B and S1C). All synthesized ligands were characterized using $^{1}$H nuclear magnetic resonance (NMR; Fig. S1 to S3) spectroscopy and high-resolution mass spectrometry (HRMS).

By following our previously reported method,[29] the brominated Pt(IV) complex *cis*,*trans*-[Pt$(NH_3)_2$(CBDCA)(OH)Br] was reacted with silver nitrate to yield the aquated intermediate *cis*,*trans*-[Pt$(NH_3)_2$(CBDCA)(OH)$(OH_2)$]$(NO_3)$, where CBDCA is 1,1-cyclobutanedicarboxylate. The silver bromide precipitate was filtered off before the addition of **flav-1**, resulting in the first desired Pt(IV) complex *cis*,*trans*-[Pt$(NH_3)_2$(CBDCA)(OH)(**flav-1**)]$(NO_3)$, designated flavoplatin **1a** (Fig. 1 and Scheme S2A). Similarly, starting from *cis*,*trans*-[Pt$(NH_3)_2$(CBDCA)(OH)Br], flavoplatins **2a** and **3a** were respectively synthesized through ligand exchange reactions with **flav-2** and **flav-3** (Scheme S2A). Additionally, we explored the modification of the axial hydroxido ligand of flavoplatins. Reactions of flavoplatins **2a** and **3a** with acetic anhydride converted them into *cis*,*trans*-[Pt$(NH_3)_2$(CBDCA)$(OCOCH_3)$(**flav-2**)]$(NO_3)$ (**2b**) and *cis*,*trans*-[Pt$(NH_3)_2$(CBDCA)$(OCOCH_3)$(**flav-3**)]$(NO_3)$ (**3b**), respectively, while the carboxylated product of flavoplatin **1a** was not obtained under the same condition (Fig. 1 and Scheme S2A). For the oxaliplatin-based brominated Pt(IV) complex, the ligand exchange reaction was modified by using an acetonitrile/dimethyl sulfoxide (DMSO; 3 : 1) solvent mixture. This procedure yielded another flavoplatin *trans*-[Pt(DACH)(ox)(OH)(**flav-3**)]$(NO_3)$ (**3c**), synthesized by coordinating **flav-3** to the oxaliplatin-based Pt(IV) complex (Scheme S2B). The flavoplatins were characterized by $^{1}$H, $^{13}$C, $^{195}$Pt NMR spectroscopy and HRMS (Fig. S4–S18). Their purities were confirmed by high-performance liquid chromatography (HPLC; Fig. S19).

The hydrolytic stability of flavoplatins in the dark was determined using HPLC (Fig. S20–S25). All the tested complexes displayed a half-life of over 24 h in HEPES buffer. Among them, flavoplatins **3b** and **3c** were the most stable, remaining 95% and 98% intact after 24 h of incubation, respectively (Fig. 2A). Flavoplatin **2b** also displayed moderately high stability, with 79% of the complex intact after 24 h. This suggests that the introduction of an axial acetato ligand may contribute to the stabilization of these complexes against hydrolysis. A comparison of Pt(IV) complexes bearing different flavonol ligands revealed an additional trend: **flav-3**-containing complexes were

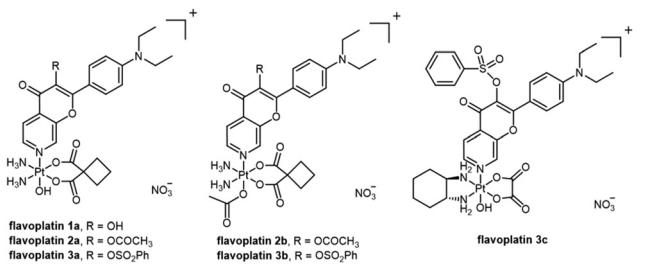


**Fig. 1** Chemical structures of flavoplatins **1a**, **2a**, **2b**, **3a**, **3b**, and **3c**.

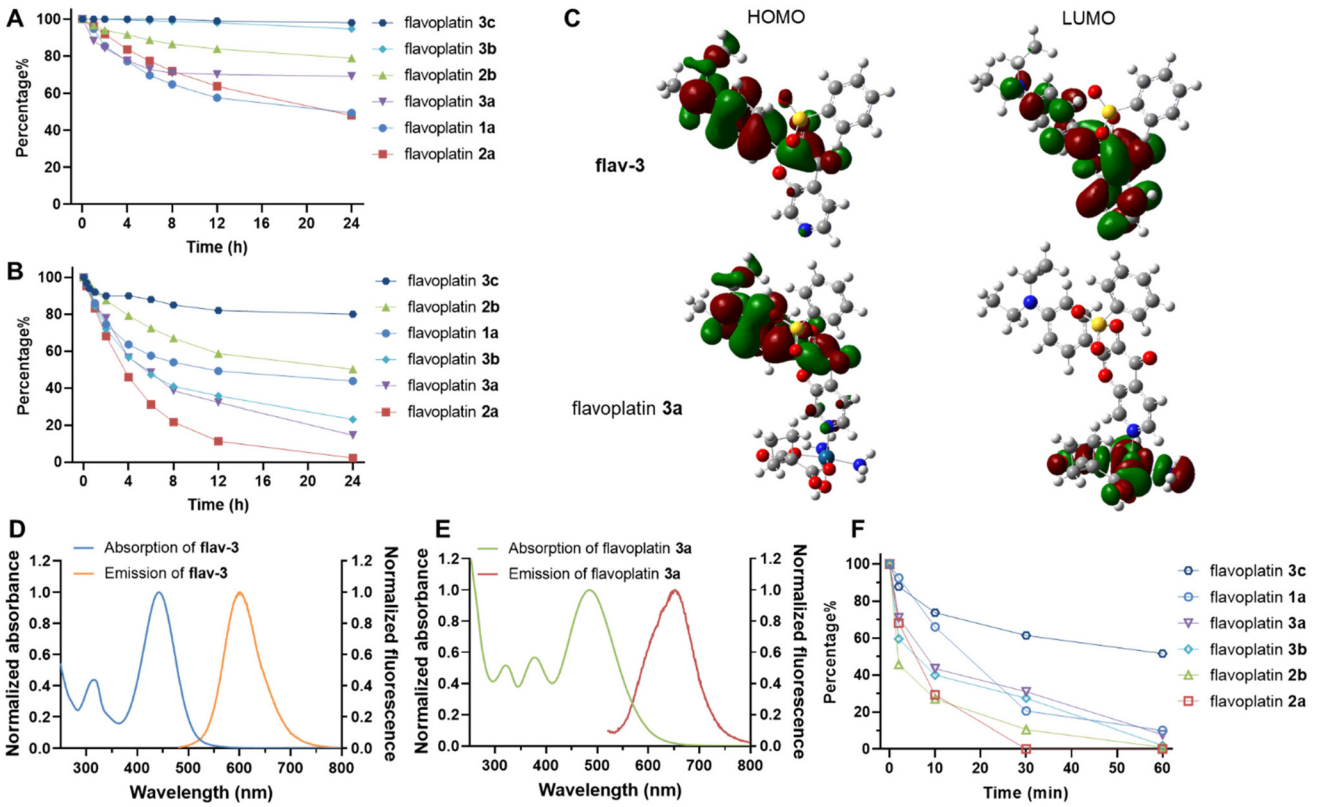


**Fig. 2** (A) and (B) Stability tests of flavoplatins **1a**, **2a**, **2b**, **3a**, **3b**, and **3c**; 200 μM flavoplatin solutions were prepared in 50 mM HEPES buffer (20% DMF, pH 7.4) and incubated at 37 °C. Solutions were monitored by HPLC from 0 to 24 h. (B) Flavoplatin solutions with 2 mM sodium ascorbate (pH 7.4) were monitored by HPLC from 0 to 24 h. (C) HOMO and LUMO of **flav-3** and flavoplatin **3a**. (D) Absorption spectrum of 25 μM **flav-3** and emission spectrum of 10 μM **flav-3** excited at 405 nm, in 50 mM HEPES buffer (20% DMF, pH 7.4). (E) Absorption spectrum of 25 μM flavoplatin **3a** and emission spectrum of 10 μM flavoplatin **3a** excited at 488 nm; in 50 mM HEPES buffer (20% DMF, pH 7.4). (F) Photoactivation tests of flavoplatins **1a**, **2a**, **2b**, **3a**, **3b**, and **3c**; 200 μM flavoplatin solutions were prepared in 50 mM HEPES buffer with 2 mM sodium ascorbate (20% DMF, pH 7.4), irradiated by a green LED (495 nm, 0.9 mW $cm^{-2}$) for 0 to 60 min at 37 °C, and immediately monitored by HPLC.

more stable than those bearing **flav-1** or **flav-2** ligands (**3b** > **2b**; **3a** > **1a** > **2a**). The hydrolysis products of the flavoplatins were analyzed by liquid chromatography-mass spectrometry (LC-MS). During hydrolysis, the **flav-1** and **flav-3** ligands were released from flavoplatins **1a** and **3a**, respectively (Fig. S20 and S23). In contrast, the N–Pt bond in flavoplatin **2a** remained stable, with hydrolysis leading instead to cleavage of the acetate group from the **flav-2** ligand (Fig. S21).

We conducted additional tests to assess the stability of flavoplatins in the presence of sodium ascorbate (Fig. 2B and S26–S31). Flavoplatin **3c** exhibited the highest stability, with over 80% remaining after 24 h, followed by flavoplatins **2b** (51%) and **1a** (44%, Table S1). The other flavoplatins displayed moderate stability in the presence of the reducing agent, with a half-life of approximately 4 h (**2a**, 3.7 h; **3a**, 4.2 h; **3b**, 4.4 h; Fig. 2B and Table S1). The reduction products of all tested complexes were analyzed using HRMS. Flavoplatins are predominantly reduced to carboplatin or oxaliplatin, releasing the corresponding axial flavonol ligands (Fig. S32). During reduction, the hydrolysis of the acetate group in flavoplatin **2a** occurred, resulting in the minor product ligand **flav-1** (Fig. S27). Intriguingly, reductive ligand rearrangements were observed in flavoplatins **1a**, **3a**, and **3b**; in these cases, the flavonol ligands remained intact; through the loss of an amine and the axial hydroxido or acetato ligand, a class of flavonol-bearing Pt(II) complexes was formed as minor products (Fig. S26, S29, and S30).

To investigate the excitation profiles of the flavonol ligands and flavoplatins, we selected **flav-3** and flavoplatin **3a** for computational analysis. Time-dependent density functional theory (TD-DFT) calculations showed that the lowest singlet excited state ($S_1$) in both species was primarily dominated by a HOMO to LUMO transition. For **flav-3**, both frontier orbitals reside largely on the ligand, consistent with a typical intra-ligand (IL) excitation. In contrast, for flavoplatin **3a**, the HOMO was mainly distributed on the flav-3 ligand, whereas the LUMO was centered on the Pt(IV) moiety, indicating pronounced ligand-to-metal charge transfer (LMCT). This strong LMCT character reduced the $S_0$ to $S_1$ energy gap following the conjugation of **flav-3** ($\Delta E$ = 2.87 eV, $\lambda$ = 432 nm) to the Pt(IV) center (flavoplatin **3a**: $\Delta E$ = 2.33 eV, $\lambda$ = 533 nm; Table S2). This decrease resulted in absorption at longer wavelengths. Consistent with computations, flavoplatin **3a** exhibited a significant red shift in the experimental absorption maximum

($\lambda_{max}$ = 484 nm) compared with **flav-3** ($\lambda_{max}$ = 442 nm; Fig. 2D and E), supporting the presence of an LMCT band driven by aromatic *N*-coordination. Consequently, we employed a blue LED ($\lambda_{max}$ = 425 nm, 1.0 mW cm$^{-2}$) to investigate the photoactivation profiles of ligands **flav-1** to **flav-3**, and a green LED ($\lambda_{max}$ = 495 nm, 0.9 mW cm$^{-2}$) for flavoplatins **1a** to **3c** (Fig. S33). Furthermore, we recorded the emission spectra of **flav-3** and flavoplatin **3a**, with the fluorescence wavelengths centered at 601 nm and 653 nm, respectively (Fig. 2D and E).

The activation of flavoplatins in HEPES buffer under green light irradiation was monitored using HPLC, and the photoreaction quantum yield was calculated and presented in Table S3. Most flavoplatins were efficiently activated within 1 h of irradiation (Fig. 2F). Flavoplatin **3c** exhibited lower activation efficiency, with 52% remaining intact in the buffer after exposure. During the photoactivation process, flavoplatins were reduced to carboplatin and oxaliplatin, with the detachment of flavonol ligands **flav-1**, **flav-2**, and **flav-3** (Fig. S34–S35, Scheme S3).

Next, we tested the cytotoxicity of flavoplatins and the corresponding ligands against ovarian cancer cells, as well as the mixture of Pt(II) drugs and the ligands (Fig. 3 and Table S3). As controls, cisplatin, carboplatin, and oxaliplatin showed no light-dependent change in cytotoxicity, although cisplatin and oxaliplatin displayed moderate cytotoxicity in Pt-sensitive cells (Table S4). Under blue light irradiation, ligands **flav-1** and **flav-2** demonstrated up to an 11.7-fold increase in cytotoxicity relative to dark conditions. A 1 : 1 mixture of **flav-1** and carboplatin produced comparable photocytotoxicities in A2780 and A2780cisR cells, yielding a low resistance factor (RF) of 1.1. Similarly, the mixtures of **flav-3** with carboplatin or oxaliplatin also reduced resistance upon irradiation (RFs 1.0 and 1.1). Under green-light irradiation, the Pt(IV) prodrug flavoplatin **1a** exhibited $IC_{50}$ values of 79.3 μM and 84.3 μM against A2780 and A2780cisR cells, respectively, with a low RF of 1.1 (Fig. 3 and Table S3), whereas flavoplatins **2a** and **2b** were not photocytotoxic. In contrast, green-light-activated flavoplatins **3a** and **3b** achieved $IC_{50}$ values of 14.2–18.3 μM (PI > 5.4) in A2780 and A2780cisR cells, with RFs as low as 0.8, representing >35-fold greater photocytotoxicity than carboplatin and up to 20-fold greater than the **flav-3**/carboplatin mixture. The oxaliplatin-based flavoplatin **3c** was also active under green light irradiation and reduced drug resistance. Overall, flavoplatins **1a** and **3a** to **3c** showed enhanced cytotoxicity under green-light irradiation, whereas the free flavonol ligands are preferentially activated by blue light, aligning with their maximum absorption wavelength. Notably, the sulfonated flavonol-derived ligand **flav-3** acted as a robust photosensitive ligand for Pt(IV) prodrugs, making flavoplatins **3a** to **3c** promising candidates for further investigation into their mechanisms of action.

We subsequently evaluated the cellular accumulation and genomic DNA binding levels of the flavoplatins. Compared to carboplatin, flavoplatin **3a** exhibited a 5.6-fold higher accumulation level in A2780cisR cells. Similarly, flavoplatins **1a**, **3b**, and **3c** displayed 2.4- to 2.7-fold increases in accumulation levels relative to their parent Pt(II) drugs (Fig. 4A). Without irradiation, the levels of Pt in the genomic DNA of cells treated with flavoplatins **1a**, **3a**, **3b**, and **3c** were compar-

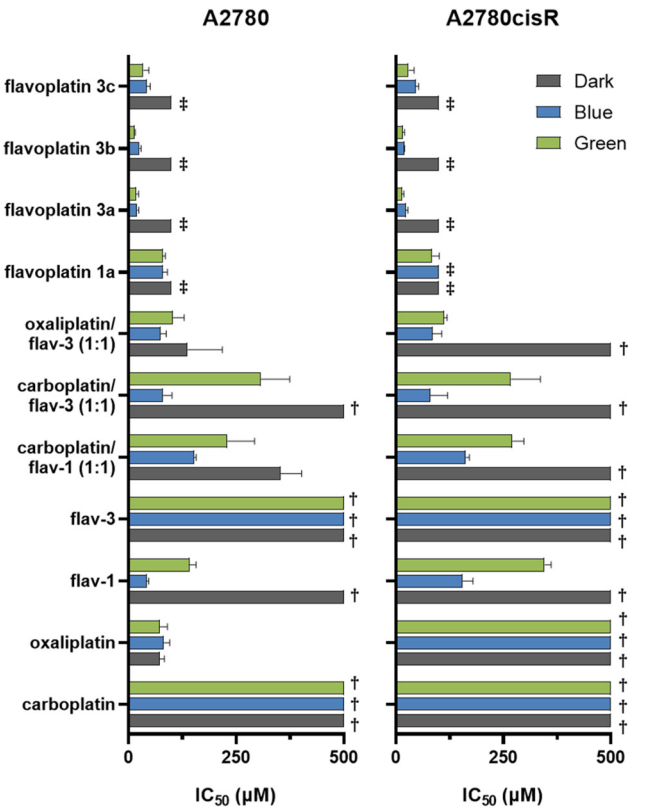


**Fig. 3** Photo-cytotoxicity assays in A2780 and A2780cisR cells, which were treated with the compounds for 2 h, followed by blue light (425 nm, 1.0 mW cm$^{-2}$) or green light irradiation (495 nm, 0.9 mW cm$^{-2}$) for 1 h. The cells were incubated for another 21 h before the MTT assays, with the total treatment time being 24 h. †$IC_{50}$ > 500 μM; ‡$IC_{50}$ > 100 μM.

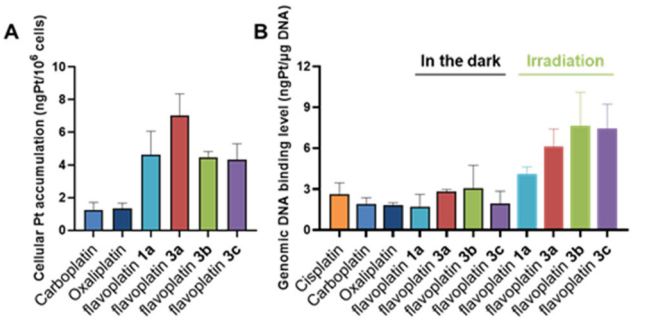


**Fig. 4** (A) Pt accumulation levels in A2780cisR cells treated with 20 μM carboplatin, oxaliplatin, and flavoplatins **1a**, **3a**, **3b**, and **3c** for 2 h. (B) Genomic DNA binding levels of A2780cisR cells treated for 2 h with 50 μM flavoplatins **1a**, **3a**, **3b**, and **3c**, followed by green light irradiation (495 nm, 0.9 mW cm$^{-2}$) for 1 h, and the total treatment time was 24 h. The cells treated with 50 μM cisplatin, carboplatin, and oxaliplatin for 24 h in the dark were included as the positive controls.

able to those observed with Pt(II) drugs (Fig. 4B). In contrast, these levels of Pt increased by 1.8- to 2.5-fold under green light irradiation, demonstrating that these Pt(IV) prodrugs, including flavoplatin **3c**, were activated efficiently in the cells. Additionally, the ability of flavoplatins to damage DNA under irradiation was confirmed by the increased expression levels of γ-H2AX in A2780cisR cells (Fig. S36).

After evaluating cellular accumulation and genomic DNA binding levels, we carried out cell cycle arrest and PI/annexin V double staining assays to determine the mode of cell death induced by flavoplatins. Cisplatin arrested the cancer cells in the S phase. In contrast, upon green light irradiation, flavoplatins **1a**, **3a**, **3b**, and **3c** arrested A2780cisR cells in the $G_2$/M phase (Fig. 5A and S37). Moreover, flavoplatins **3a**, **3b**, and **3c** significantly increased the percentage of cells in late apoptosis and late necrosis, while compared to cisplatin and oxaliplatin, fewer cells remained in early apoptosis (Fig. 5B and S38). These results suggest that flavoplatins **3a**, **3b**, and **3c** exhibit a different mechanism of action compared to the conventional platinum drugs.

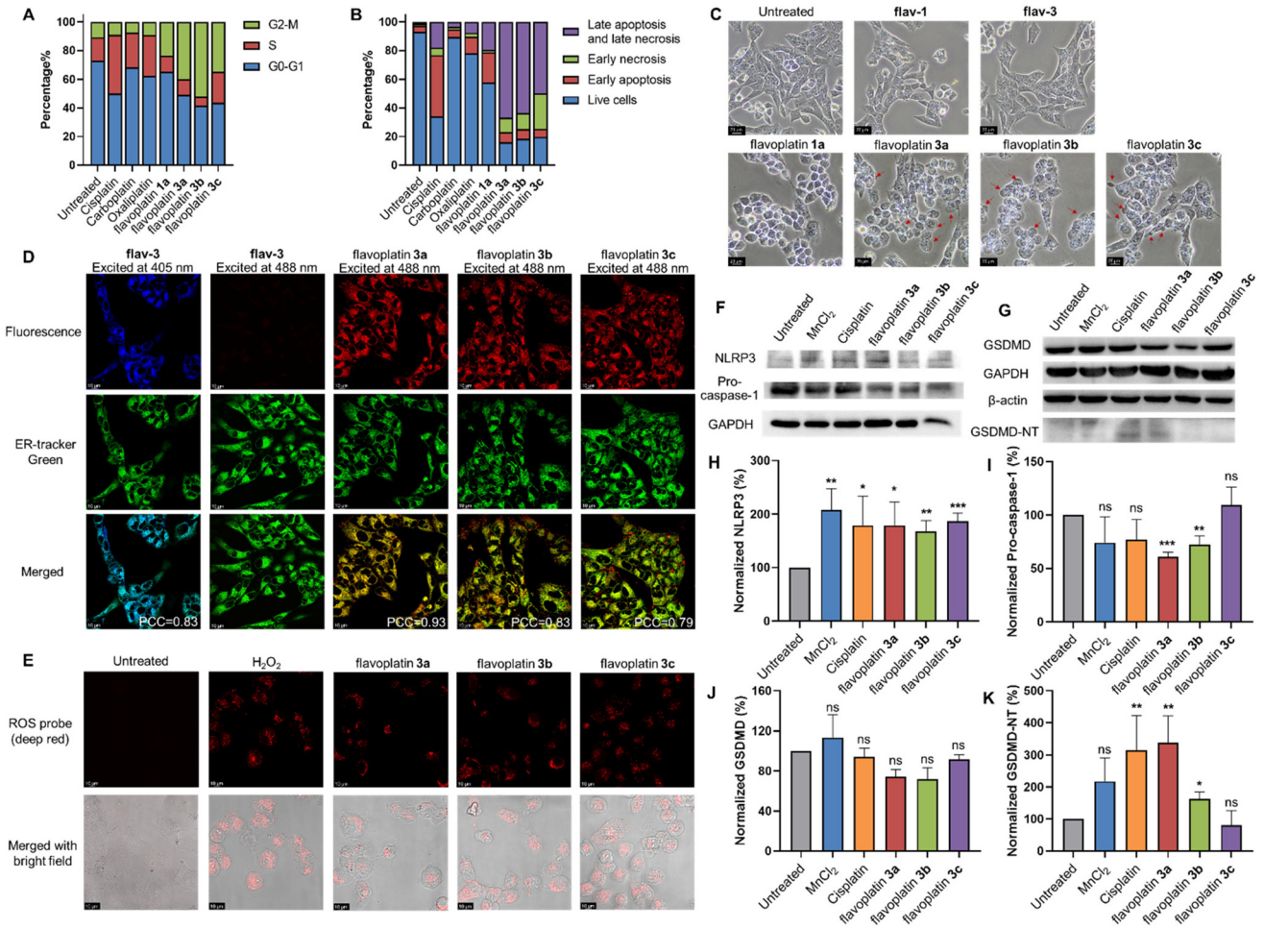


**Fig. 5** (A) Cell cycle arrest and (B) apoptotic cells analysis of A2780cisR cells treated for 2 h with 50 μM flavoplatins **1a**, **3a**, **3b**, and **3c**, followed by green light irradiation (495 nm, 0.9 mW $cm^{-2}$) for 1 h, and the total treatment time was 5 h. The cells treated with 200 μM cisplatin, carboplatin, and oxaliplatin for 5 h in the dark were included as the positive controls. (C) Cell morphology of A2780cisR cells treated with 100 μM **flav-1** and **flav-3** for 2 h, and 50 μM flavoplatins **1a**, **3a**, **3b**, and **3c** for 2 h. The treated cells were irradiated by green light (495 nm, 0.9 mW $cm^{-2}$) for 1 h, while the untreated group was kept in the dark. Scale bar represents 20 μm. (D) Co-localization of ER tracker green and flavoplatins in A2780cisR cells, treated with 25 μM flavoplatins **3a**, **3b**, and **3c**, as well as 25 μM **flav-3** for 2 h. Cells were imaged by a Laser Confocal Scanning Microscope; blue channel was excited at 405 nm, emission was recorded at 570 to 630 nm; green channel was excited at 488 nm, emissions were recorded at 500 to 520 nm and 625 to 675 nm. Scale bar represents 10 μm. (E) Fluorescence of a ROS probe (deep red) with the excitation at 635 nm, and emission was recorded at 660 to 680 nm. A2780cisR cells treated with 50 μM flavoplatins **3a**, **3b**, and **3c** for 2 h. The flavoplatin-treated cells were irradiated by green light (495 nm, 0.9 mW $cm^{-2}$) for 30 min, while the untreated cells were kept in the dark. Scale bar represents 10 μm. Western blotting images of (F) NLRP3 and pro-caspase-1, as well as (G) GSDMD and its N-terminal fragments. A2780cisR cells were treated with 50 μM flavoplatins **3a**, **3b**, and **3c** for 2 h. The flavoplatin-treated cells were irradiated by green light (495 nm, 0.9 mW $cm^{-2}$) for 1 h, while the untreated cells were kept in the dark. The cells treated with 1 mM $MnCl_2$ and 200 μM cisplatin for 4 h in the dark were included as the positive controls. The representative results were selected from three independent experiments. (H) Quantified expression levels of NLRP3; (I) pro-caspase-1; (J) GSDMD, and (K) GSDMD N-terminal fragment. *** $p \leq 0.001$, ** $p \leq 0.01$, * $0.01 < p \leq 0.05$, ns: not significant.

To further study the mechanisms of action, the morphologies of cells treated with flavoplatins and subjected to irradiation were imaged and analyzed. The presence of pyroptotic bodies and cell swelling in A2780cisR cells treated with flavoplatins **3a** to **3c** suggested that the mode of cell death was likely pyroptosis (Fig. 5C). Since the pyroptotic pathways involving ER oxidative stress have been documented,[44,45] we subsequently investigated the ER targeting ability and ROS generation of flavoplatins. Intracellular imaging was carried out in the A2780cisR cells treated with flavoplatins and **flav-3**, after incubation with a fluorescent ER tracker. Ligand **flav-3** in the cells emitted intense fluorescence upon the excitation of blue light (405 nm; Fig. 2D and 5D), while flavoplatins **3a**, **3b**, and **3c** were excited by green light (488 nm) and fluorescent (Fig. 2E and 5D). These observations revealed that the free ligand **flav-3** and the Pt(IV) complexes could be distinguished by different excitation wavelengths of light. Notably, the sulfonated flavoplatins **3a**, **3b**, and **3c**, as well as the free ligand **flav-3**, colocalized well with the ER tracker, with Pearson correlation coefficients (PCCs) ranging from 0.79 to 0.93 (Fig. 5D). In contrast, flavoplatin **1a**, which was a sulfonate-free Pt(IV) complex, did not target the ER (Fig. S39). Additionally, flavoplatins **3a**, **3b**, and **3c** upon irradiation generated ROS in the cells (Fig. 5E and S40), demonstrating these Pt(IV) prodrugs likely trigger ER oxidative stress.

Finally, we assessed the expression levels of proteins involved in ER stress pathways, including NLRP3 inflammasome,[44,45] to confirm the pyroptosis induced by flavoplatins **3a** to **3c**. Gasdermin D (GSDMD) and gasdermin E (GSDME) are essential proteins involved in pyroptosis, responsible for membrane pore formation following cleavage by caspases.[46] We subsequently evaluated the NLPR3/caspase-1/GSDMD pathway in A2780cisR cells treated with flavoplatins and irradiated (Fig. 5F and G), using cisplatin and a manganese salt as controls, as they have been reported to trigger GSDMD cleavage through certain mechanisms.[47,48] The results demonstrated that flavoplatins **3a** **3b**, and **3c** effectively increased the expression of NLRP-3 (Fig. 5H), in which flavoplatins **3a** and **3b** further decreased the levels of downstream pro-caspase-1 by 39% and 28%, respectively (Fig. 5I). Notably, over 3-fold increased expression of the GSDMD N-terminus was observed in flavoplatin **3a**-treated groups, with the levels of GSDMD decreased by 26% (Fig. 5J and K). The cleavage of GSDMD was also observed in the cisplatin- and manganese-treated groups, aligning with previous reports.[47,48] Next, we examined the caspase-3/GSDME pathway by blotting the corresponding proteins, and a doxorubicin-treated group was included as a control (Fig. S41). The results showed that only doxorubicin effectively activated caspase-3 and degraded GSDME. The N-terminal of GSDME, which is responsible for pore formation, was observed in doxorubicin-treated cells but not in flavoplatin-treated cells.[49] These findings indicate that flavoplatins **3a** and **3b**, upon irradiation, actively induced pyroptosis in A2780cisR cells *via* the NLPR3/caspase-1/GSDMD pathway. These Pt(IV) prodrugs are distinct from conventional apoptosis-inducing Pt(II) drugs and provide an approach to overcoming Pt-drug resistance.

## Conclusions

In summary, we developed a series of photoactivable Pt(IV) anticancer prodrugs by conjugating flavonol-derived ligands to Pt(IV) complexes through *N*-coordination. This approach enhanced LMCT and enabled activation using green light. Upon light irradiation, most of these Pt(IV) complexes were quickly reduced to either carboplatin or oxaliplatin. The sulfonate-containing flavoplatins **3a**, **3b**, and **3c** efficiently accumulated in the ER and effectively killed platinum-resistant cancer cells when irradiated, exhibiting high photo-indexes. Following the observation of pyroptotic cell morphologies and ROS generation, the NLRP3/caspase-1/GSDMD pathway of pyroptosis was confirmed. This work introduces a novel strategy for designing photoactivable Pt(IV) prodrugs, significantly improving cytotoxicity compared to non-irradiated conditions and reducing drug resistance by inducing pyroptosis. Extending the excitation wavelength through N coordination offers a route to near-infrared (NIR)-activatable Pt(IV) prodrugs.

## Author contributions

Q. Z. and G. Z. designed the study. Q. Z. and N.-H. C. performed the experiments. J. X. performed the DFT calculations. Q. Z., K.-C. L. and G. Z. analyzed the data. Q. Z. and G. Z. wrote the paper. All authors edited and approved the final manuscript.

## Conflicts of interest

There are no conflicts to declare.

## Data availability

The data supporting this article (Instruments and methods, Experimental sections, Schemes S1 to S3, Fig. S1 to S43, and Tables S1 to S4) have been included as part of the supplementary information (SI). Supplementary information is available. See DOI: **https://doi.org/10.1039/d6qi00078a**.

## Acknowledgements

We thank the National Natural Science Foundation of China (Grant No. 22077108 and 22277103), the Hong Kong Research Grants Council (Grant No. CityU 11313222, CityU 11304923, CityU 11306724, and CityU C1018-23G), the Science Technology and Innovation Committee of Shenzhen Municipality (JCYJ20210324120004011), and the City

 

University of Hong Kong (Grant No. 9610605) for funding support.

## References

1 A. N. Panche, A. D. Diwan and S. R. Chandra, Flavonoids: an overview, *J. Nutr. Sci.*, 2016, **5**, e47.
2 E. G. Schijlen, C. R. De Vos, A. J. van Tunen and A. G. Bovy, Modification of flavonoid biosynthesis in crop plants, *Phytochemistry*, 2004, **65**, 2631–2648.
3 S. Kumar and A. K. Pandey, Chemistry and biological activities of flavonoids: an overview, *Sci. World J.*, 2013, **2013**, 162750.
4 E. Middleton Jr, Effect of plant flavonoids on immune and inflammatory cell function, *Adv. Exp. Med. Biol.*, 1998, **439**, 175–182.
5 D. M. Kopustinskiene, V. Jakstas, A. Savickas and J. Bernatoniene, Flavonoids as anticancer agents, *Nutrients*, 2020, **12**, 457.
6 P. Batra and A. K. Sharma, Anti-cancer potential of flavonoids: recent trends and future perspectives, *3 Biotech*, 2013, **3**, 439–459.
7 A. Rauf, M. Imran, I. A. Khan, M. ur-Rehman, S. A. Gilani, Z. Mehmood and M. S. Mubarak, Anticancer potential of quercetin: a comprehensive review, *Phytother. Res.*, 2018, **32**, 2109–2130.
8 T. Okamoto, Safety of quercetin for clinical application, *Int. J. Mol. Med.*, 2005, **16**, 275–278.
9 X. Wang, Y. Yang, Y. An and G. Fang, The mechanism of anticancer action and potential clinical use of kaempferol in the treatment of breast cancer, *Biomed. Pharmacother.*, 2019, **117**, 109086.
10 T. Rengarajan and N. S. Yaacob, The flavonoid fisetin as an anticancer agent targeting the growth signaling pathways, *Eur. J. Pharmacol.*, 2016, **789**, 8–16.
11 K. P. Devi, T. Rajavel, S. Habtemariam, S. F. Nabavi and S. M. Nabavi, Molecular mechanisms underlying anticancer effects of myricetin, *Life Sci.*, 2015, **142**, 19–25.
12 L. McDonald, B. Liu, A. Taraboletti, K. Whiddon, L. P. Shriver, M. Konopka, Q. Liu and Y. Pang, Fluorescent flavonoids for endoplasmic reticulum cell imaging, *J. Mater. Chem. B*, 2016, **4**, 7902–7908.
13 L. S. Lazarus, C. T. Dederich, S. N. Anderson, A. D. Benninghoff and L. M. Berreau, Flavonol-based carbon monoxide delivery molecule with endoplasmic reticulum, mitochondria, and lysosome localization, *ACS Med. Chem. Lett.*, 2022, **13**, 236–242.
14 Y. Shi, S. Wang, J. Wu, X. Jin and J. You, Pharmaceutical strategies for endoplasmic reticulum-targeting and their prospects of application, *J. Controlled Release*, 2021, **329**, 337–352.
15 X. Bi, B. Liu, L. McDonald and Y. Pang, Excited-state intramolecular proton transfer (ESIPT) of fluorescent flavonoid dyes: A close look by low temperature fluorescence, *J. Phys. Chem. B*, 2017, **121**, 4981–4986.
16 M. Tian, J. Sun, Y. Tang, B. Dong and W. Lin, Discriminating live and dead cells in dual-color mode with a two-photon fluorescent probe based on ESIPT mechanism, *Anal. Chem.*, 2018, **90**, 998–1005.
17 T. C. Johnstone, K. Suntharalingam and S. J. Lippard, The next generation of platinum drugs: targeted Pt(II) agents, nanoparticle delivery, and Pt(IV) prodrugs, *Chem. Rev.*, 2016, **116**, 3436–3486.
18 M. D. Hall, H. R. Mellor, R. Callaghan and T. W. Hambley, Basis for design and development of platinum(IV) anticancer complexes, *J. Med. Chem.*, 2007, **50**, 3403–3411.
19 D. Gibson, Platinum(IV) anticancer prodrugs–hypotheses and facts, *Dalton Trans.*, 2016, **45**, 12983–12991.
20 A. Lopez-Sanchez and H. Bertrand, Pt(IV) anticancer prodrugs bearing an oxaliplatin scaffold: what do we know about their bioactivity?, *Inorg. Chem. Front.*, 2024, **11**, 1639–1667.
21 J. J. Wilson and S. J. Lippard, Synthetic methods for the preparation of platinum anticancer complexes, *Chem. Rev.*, 2014, **114**, 4470–4495.
22 F. Navas, A. Chocarro-Calvo, P. Iglesias-Hernández, P. Fernández-García, V. Morales, J. M. García-Martínez, R. Sanz, A. De la Vieja, C. García-Jiménez and R. A. García-Muñoz, Promising anticancer prodrugs based on Pt(IV) complexes with bis-organosilane ligands in axial positions, *J. Med. Chem.*, 2024, **67**, 6410–6424.
23 O. O. Krasnovskaya, R. A. Akasov, D. V. Spector, K. G. Pavlov, A. A. Bubley, V. A. Kuzmin, A. A. Kostyukov, E. V. Khaydukov, E. V. Lopatukhina, A. S. Semkina, K. Yu. Vlasova, S. A. Sypalov, A. S. Erofeev, P. V. Gorelkin, A. N. Vaneev, V. N. Nikitina, D. A. Skvortsov, D. A. Ipatova, D. M. Mazur, N. V. Zyk, D. A. Sakharov, A. G. Majouga and E. K. Beloglazkina, Photoinduced reduction of novel dual-action riboplatin Pt(IV) prodrug, *ACS Appl. Mater. Interfaces*, 2023, **15**, 12882–12894.
24 J. Sánchez-Camacho, S. Infante-Tadeo, A. C. Carrasco, S. Scoditti, Á. Martínez, F. Barroso-Bujans, E. Sicilia, A. M. Pizarro and L. Salassa, Flavin-conjugated Pt(IV) anticancer agents, *Inorg. Chem.*, 2023, **62**, 5644–5651.
25 S. Jin, N. Muhammad, Y. Sun, Y. Tan, H. Yuan, D. Song, Z. Guo and X. Wang, Multispecific platinum(IV) complex deters breast cancer via interposing inflammation and immunosuppression as an inhibitor of COX-2 and PD-L1, *Angew. Chem.*, 2020, **132**, 23513–23521.
26 G. Thiabaud, G. He, S. Sen, K. A. Shelton, W. B. Baze, L. Segura, J. Alaniz, R. Munoz Macias, G. Lyness, A. B. Watts, H. M. Kim, H. Lee, M. Y. Cho, K. S. Hong, R. Finch, Z. H. Siddik, J. F. Arambula and J. L. Sessler, Oxaliplatin Pt(IV) prodrugs conjugated to gadolinium-texaphyrin as potential antitumor agents, *Proc. Natl. Acad. Sci. U. S. A.*, 2020, **117**, 7021–7029.
27 G. Pelosi, M. Ravera, E. Gabano, F. Fregonese and D. Osella, Unprecedented one-pot synthesis of an unsymmetrical cisplatin-based Pt(IV)-acetamidato complex, *Chem. Commun.*, 2015, **51**, 8051–8053.

28 M. Ravera, E. Gabano, I. Zanellato, F. Fregonese, G. Pelosi, J. A. Platts and D. Osella, Antiproliferative activity of a series of cisplatin-based Pt(IV)-acetylamido/carboxylato prodrugs, *Dalton Trans.*, 2016, **45**, 5300–5309.

29 Q. Zhou, S. Chen, Z. Xu, G. Liu, S. Zhang, Z. Wang, M. K. Tse, S. M. Yiu and G. Zhu, Multitargeted platinum(IV) anticancer complexes bearing pyridinyl ligands as axial leaving groups, *Angew. Chem., Int. Ed.*, 2023, **62**, e202302156.

30 J. Huang, W. Ding, X. Zhu, B. Li, F. Zeng, K. Wu, X. Wu and F. Wang, Ligand evolution in the photoactivatable platinum(IV) anticancer prodrugs, *Front. Chem.*, 2022, **10**, 876410.

31 N. A. Kratochwil, M. Zabel, K.-J. Range and P. J. Bednarski, Synthesis and X-ray crystal structure of *trans*,*cis*-[Pt$(OAc)_2I_2$(en)]: a novel type of cisplatin analog that can be photolyzed by visible light to DNA-binding and cytotoxic species in vitro, *J. Med. Chem.*, 1996, **39**, 2499–2507.

32 F. S. Mackay, J. A. Woods, H. Moseley, J. Ferguson, A. Dawson, S. Parsons and P. J. Sadler, A photoactivated *trans*-diammine platinum complex as cytotoxic as cisplatin, *Chem. – Eur. J.*, 2006, **12**, 3155–3161.

33 L. Brancaleon and H. Moseley, Laser and non-laser light sources for photodynamic therapy, *Lasers Med. Sci.*, 2002, **17**, 173–186.

34 N. J. Farrer, J. A. Woods, L. Salassa, Y. Zhao, K. S. Robinson, G. Clarkson, F. S. Mackay and P. J. Sadler, A potent *trans*-diimine platinum anticancer complex photoactivated by visible light, *Angew. Chem.*, 2010, **122**, 9089–9092.

35 H. Yao, S. Chen, Z. Deng, M.-K. Tse, Y. Matsuda and G. Zhu, BODI-Pt, a green-light-activatable and carboplatin-based platinum(IV) anticancer prodrug with enhanced activation and cytotoxicity, *Inorg. Chem.*, 2020, **59**, 11823–11833.

36 Z. Wang, N. Wang, S.-C. Cheng, K. Xu, Z. Deng, S. Chen, Z. Xu, K. Xie, M.-K. Tse, P. Shi, H. Hirao, C.-C. Ko and G. Zhu, Phorbiplatin, a highly potent Pt(IV) antitumor prodrug that can be controllably activated by red light, *Chem*, 2019, **5**, 3151–3165.

37 Z. Deng, H. Li, S. Chen, N. Wang, G. Liu, D. Liu, W. Ou, F. Xu, X. Wang, D. Lei, P.-C. Lo, Y. Li, J. Lu, M. Yang, M.-L. He and G. Zhu, Near-infrared-activated anticancer platinum(IV) complexes directly photooxidize biomolecules in an oxygen-independent manner, *Nat. Chem.*, 2023, **15**, 930–939.

38 M. Imran, W. Ayub and I. S. Butler, Photoactivated platinum-based anticancer drugs, *Coord. Chem. Rev.*, 2018, **376**, 405–429.

39 Z. Deng, N. Wang, Y. Liu, Z. Xu, Z. Wang, T.-C. Lau and G. Zhu, A photocaged, water-oxidizing, and nucleolus-targeted Pt(IV) complex with a distinct anticancer mechanism, *J. Am. Chem. Soc.*, 2020, **142**, 7803–7812.

40 H. Shi, R. C. Marchi and P. J. Sadler, Advances in the design of photoactivatable metallodrugs: excited state metallomics, *Angew. Chem., Int. Ed.*, 2025, **64**, e202423335.

41 F. S. Mackay, S. A. Moggach, A. Collins, S. Parsons and P. J. Sadler, Photoactive trans ammine/amine diazido platinum(IV) complexes, *Inorg. Chim. Acta*, 2009, **362**, 811–819.

42 F. Juliá, Ligand-to-metal charge transfer (LMCT) photochemistry at 3d-metal complexes: an emerging tool for sustainable organic synthesis, *ChemCatChem*, 2022, **14**, e202200916.

43 H. C. Tai, Y. Zhao, N. J. Farrer, A. E. Anastasi, G. Clarkson, P. J. Sadler and R. J. Deeth, A computational approach to tuning the photochemistry of platinum(IV) anticancer agents, *Chem. – Eur. J.*, 2012, **18**, 10630–10642.

44 H. Kato and H. Nishitoh, Stress responses from the endoplasmic reticulum in cancer, *Front. Oncol.*, 2015, **5**, 93.

45 S. Zeng, C. Chen, L. Zhang, X. Liu, M. Qian, H. Cui, J. Wang, Q. Chen and X. Peng, Activation of pyroptosis by specific organelle-targeting photodynamic therapy to amplify immunogenic cell death for anti-tumor immunotherapy, *Bioact. Mater.*, 2023, **25**, 580–593.

46 J. Shi, W. Gao and F. Shao, Pyroptosis: gasdermin-mediated programmed necrotic cell death, *Trends Biochem. Sci.*, 2017, **42**, 245–254.

47 X. Shen, H. Wang, C. Weng, H. Jiang and J. Chen, Caspase 3/GSDME-dependent pyroptosis contributes to chemotherapy drug-induced nephrotoxicity, *Cell Death Dis.*, 2021, **12**, 186.

48 H. Yan, B. Luo, X. Wu, F. Guan, X. Yu, L. Zhao, X. Ke, J. Wu and J. Yuan, Cisplatin induces pyroptosis via activation of MEG3/NLRP3/caspase-1/GSDMD pathway in triple-negative breast cancer, *Int. J. Biol. Sci.*, 2021, **17**, 2606.

49 R. Zhang, C. Wang, Y. Guan, X. Wei, M. Sha, M. Yi, M. Jing, M. Lv, W. Guo, J. Xu, Y. Wan, X.-M. Jia and Z. Jiang, Manganese salts function as potent adjuvants, *Cell. Mol. Immunol.*, 2021, **18**, 1222–1234.

 